Polymer-Enhanced Stability of Inorganic Perovskite Nanocrystals and Their Application in Color Conversion LEDs

Michaela Meyns,[†] Mariano Perálvarez,[†] Amelie Heuer-Jungemann,[⊥] Wim Hertog,[†] Maria Ibáñez,[§,‖] Raquel Nafria,[†] Aziz Genç,[¶,‖] Jordi Arbiol,[¶,¥] Maksym V. Kovalenko,[§,‖] Josep Carreras,[†,*] Andreu Cabot,[†,¥,*] Antonios G. Kanaras[⊥,*]

[†] Catalonia Institute for Energy Research - IREC, Sant Adrià de Besòs, Barcelona, 08930, Spain.

[⊥] Physics and Astronomy, Faculty of Physical Sciences and Engineering, University of Southampton, Highfield, Southampton, SO17 1BJ, U.K.

[‖] Metallurgy and Materials Engineering Department, Faculty of Engineering, Bartin University, 74100, Bartin, Turkey

[¶] Catalan Institute of Nanoscience and Nanotechnology (ICN2), CSIC and The Barcelona Institute of Science and Technology (BIST), Campus UAB, Bellaterra, 08193 Barcelona, Spain.

[¥] ICREA, Pg. Lluís Companys 23, 8010 Barcelona, Spain.

§ Institute of Inorganic Chemistry, Department of Chemistry and Applied Biosciences, ETH Zürich, CH-8093, Switzerland

‖ Empa-Swiss Federal Laboratories for Materials Science and Technology, Dübendorf, CH-8600, Switzerland

ABSTRACT

Cesium lead halide ($CsPbX_3$, X = Cl, Br, I) nanocrystals (NCs) offer exceptional optical properties for several potential applications but their implementation is hindered by a low chemical and structural stability and limited processability. In the present work, we developed a new method to efficiently coat $CsPbX_3$ NCs, which resulted in their increased chemical and optical stability as well as processability. The method is based on the incorporation of poly(maleic anhydride-*alt*-1-octadecene) (PMA) into the synthesis of the perovskite NCs. The presence of PMA in the ligand shell stabilizes the NCs by tightening the ligand binding, limiting in this way the NC surface interaction with the surrounding media. We further show that these NCs can be embedded in self-standing silicone/glass plates as down-conversion filters for the fabrication of monochromatic green and white light emitting diodes (LEDs) with narrow bandwidths and appealing color characteristics.

Keywords: Inorganic perovskite nanocrystals, $CsPbBr_3$, LED, color conversion, poly(maleic anhydride-*alt*-1-octadecene)

*Corresponding authors

Josep Carreras: jcarreras@irec.cat

Andreu Cabot: acabot@irec.cat

Antonios Kanaras: a.kanaras@soton.ac.uk

1. Introduction

Inorganic lead halide perovskite NCs with high luminescence quantum yields (up to >90%), extremely narrow emission bandwidths (< 50 nm), broad emission spectra tunability (from 410 to 700 nm) and short radiative lifetimes (<30 ns) have very recently emerged as a new class of material with outstanding potential for optoelectronic applications such as LEDs, lasing and photodetection.[1–4] Of high interest are their remarkable optical properties such as non-linear absorption, stimulated emission and blinking behavior.[2,5–7] Compared to classical Cd-based chalcogenide quantum dots (QDs), $CsPbX_3$ (X = Cl, Br, I) offer a very broad and easily adjustable composition versatility together with ample options for shape control, which allow tuning of their emission wavelength throughout the whole visible spectrum.[8–14] Among other applications, such highly luminescent and spectrally tunable NCs are ideally suited to produce monochromatic and white LEDs (WLEDs).[15] In this regard, $CsPbX_3$ NCs have been utilized as the emissive layer in electroluminescent monochromatic and color conversion QD-LEDs showing exceptionally narrow emission bandwidths and thus high color quality in devices.[16–20]

However, while $CsPbX_3$ (X = Br, I) perovskite NCs can be stored in solution, maintaining their luminescence for several months, they suffer from humidity, light and temperature driven degradation in operation conditions and from a low colloidal stability with a related limited processability.[21] In part, this is associated with a highly dynamic ligand binding to the NC surface,[22] which additionally hinders the NCs' post-synthetic purification and further functionalization. When perovskite NCs with highly ionic components and high surface energies come into contact with a polar surface or solvent, they rapidly degrade to their components. Most efforts to exchange the oleic acid coating of the as prepared NCs with ligands of interest providing additional functionality, rendering them water soluble or just protecting them from degradation, inevitably result in the NC degradation. This chemical instability is the bottleneck that limits all technological applications where the NC processing into a composite or layer is required and where NCs are exposed to an external source of energy for long times. There are two basic concepts applied for stabilizing lead halide perovskite NCs for lighting applications such as color conversion WLEDs with filters down converting blue light that may also be combined. One is based on embedding the NCs post-synthetically into a polymeric matrix such as PMMA or polystyrene.[1,18,23] The second path, very recently taken is to modify or strengthen the ligand sphere post synthetically. Increased water stability was achieved by utilizing silsesquioxane to coat $CsPbX_3$ nanocrystals.[20] Passivating $CsPbBr_3$ NCs with didodecyl dimethylammonium sulfide lead to stable amplified spontaneous emission.[24] Progress towards better stabilization based on the NCs original ligands was achieved by crosslinking of the attached long-chain ligands oleic acid and oleylamine by highly energetic radiation.[19] Additionally, the interdigitation of octadecene molecules was reported to increase stability and emission properties of organohalide perovskite NCs.[25] This raised the hope that an enforced ligand sphere is able to enhance the stability of inorganic perovskite NCs.

The integration of $CsPbX_3$ NCs in color conversion instead of electroluminescent LEDs is considered a more convenient and, in terms of material stability and processability, less demanding strategy to fabricate NC LEDs. With this approach, typical problems occurring in electroluminescent LEDs such as charging and thermal stress are reduced as no current flows through the layer. Still the processability of color conversion LEDs is not straightforward. The conventional procedure to fabricate a color conversion LED using NCs as optical phosphors involves the blending of the NCs with a thermo-curable silicone resin and deposition on top of the pump LED. In this procedure, the presence of hydrophobic organic ligand and solvents hamper the polymerization of the encapsulating resin and can reduce the mechanical stability of the composite. This is especially problematic in lead halide perovskites requiring an excess of organic ligands in solution to

prevent their aggregation,[22] which would reduce their QY and introduce scattering thus decreasing light emission.[26] To overcome the hydrophobicity limitation and improve dispersion, ligand exchange processes, the growth of oxide shells or the encapsulation of QDs in polymers, silica or glass matrices have been used in other types of semiconductors (e.g. [27–29]). However, the limited stability and processability of perovskite NCs have so far made applying similar strategies difficult.

In order to facilitate the processing and applicability of perovskite NCs, we developed a method to produce cesium lead halide NCs with improved chemical stability and compatibility for LED encapsulation by *in situ* addition of poly(maleic anhydride-*alt*-1-octadecene) (PMA). PMA has been shown to be an ideal ligand for the encapsulation of oleic acid or oleylamine-coated inorganic NCs such as magnetic, semiconductor and gold nanoparticles.[30,31] This ligand interdigitates in the carbon chain shell that surrounds the nanoparticle offering an enhanced stability. In the case of a stable NC core, the PMA units can be further polymerized utilizing a diamine, which allows the sealing of the NC core and its transfer to polar solvents. In our experiments, PMA was introduced during the synthesis of the perovskite NCs, before the injection of the Cs-precursor, to avoid any potential disruption of the perovskite NC after its formation. We further show the application of green- and orange-red-emitting $CsPbX_3$ perovskite NCs embedded in self-standing silicone-based plates as down-conversion filters in monochromatic and WLEDs. The growth of the NCs in the presence of a protecting polymer facilitates their processing by preventing aggregation and minimizing interference with the silicone curing process while better protecting the NC surface both by preventing interaction with the media and by obstructing the ligand dynamic exchange.

2. Experimental section

Materials: $PbBr_2$ (99.999% trace metals basis), 1-octadecene (90%), oleic acid (90%), poly(maleic anhydride-*alt*-1-octadecene, PMA) (M_n: 30,000-50,000), fluorescein, rhodamine 6G and Cs_2CO_3 (99.9% trace metals basis) were purchased from Sigma Aldrich, PbI_2 (99.999+%-Pb) from Strem and oleylamine (primary amine content 80-90%) from Acros. Polastosil-2000 curing and catalyst were obtained from Silikony Polskie. Round window glass with 27 mm (green LEDs) and 28 mm in diameter (WLEDs) was obtained from Edmund optics and Thermo Scientific.

Methods: $CsPbX_3$ NCs synthesis: $CsPbX_3$ NCs were prepared following a modified procedure from that reported by Protesescu *et al.*[1] Lead halide salts (0.376 mmol, green NCs: 138 mg $PbBr_2$, orange-red NCs: 69 mg $PbBr_2$ and 87 mg PbI_2) were mixed with 1-octadecene (10 mL) and heated under vacuum (60-100 mTorr) to 90 °C for 2 hours. After switching to Ar atmosphere and heating to 120 °C, oleic acid (1.0 mL) and oleylamine (1.0 mL) were injected. When a clear solution was obtained, poly(maleic anhydride-*alt*-1-octadecene) (430 mg) was added under Ar flow. Vacuum was applied and the temperature was kept constant at 100 °C for 10 minutes. The solution was stirred vigorously (1100 rpm) while the temperature was increased to 175 °C. Once this temperature was reached, Cs-oleate solution (0.8 mL) with a temperature of 130 °C was injected swiftly using a syringe pre-warmed in an oven. This way, the Cs-oleate solution remained clear, whereas partial precipitation of the precursor was observed at lower temperatures. After 15 s the reaction was quenched by cooling with a water bath.

Purification: The reaction solution was centrifuged at a speed of 7000 rpm/6300 rcf for 15 minutes. After decantation of the supernatant and of liquid residues eluting from the resting precipitate while leaving the centrifuge tube rest atop, the NCs were transferred to the glove box and stored in Ar atmosphere for further use (these are our samples after 1 precipitation). In our experience this was not necessary for the samples with PMA but to maintain comparable conditions all samples were stored in the glove box (for an

impression of the stability of particles without and with polymer see Figure S1). If further cleaning was applied, around 65 mg of sample were dispersed in 1 mL toluene and precipitated by the addition of 0.3 mL acetonitrile and centrifugation at 10000 rpm/12857 rcf for three minutes. This was repeated two to three times.

Filter plate fabrication: Green filters were prepared by drop casting 6.6 mg of NCs in 200 µL of toluene onto window glass with 27 mm diameter and letting toluene evaporate slowly in a semi-closed petri-dish under ambient conditions. To fabricate WLEDs, dried particles of each color (Balanced LED: green 7.5 mg, orange 5.1 mg; LED with higher red/orange content: green 7.6 mg, orange 7.8 mg) were dispersed with 2 drops of hexane, mixed separately with 414 ± 5 mg of liquid silicone Polastosil-2000 and sonicated for 5 minutes. Afterwards, 31 mg of curing catalyst were added and the mixtures were stirred thoroughly. After ten minutes, the mixtures were deposited on spherical optical glass with 28 mm diameter and left to cure for 60 to 75 min. When the silicone was nearly cured another glass slide was carefully put on top of one layer for separation before the second layer containing particles of the other color was stacked on top with the silicone layer facing the stack. The stack was left to cure fully for at least ten minutes more.

Characterization: Structural and chemical characterization: X-ray diffraction analyses were carried out on Bruker AXS D8 ADVANCE X-ray diffractometer with Cu–Kα radiation (λ= 0.15406 Å). Reference patterns were calculated from crystallographic data of the cubic and orthorhombic phases reported in ref. [32] by *CaRIne* software. Size and shape of the initial NCs were examined by transmission electron microscopy (TEM) using a ZEISS LIBRA 120, operating at 120 kV. High resolution TEM (HRTEM) and scanning TEM (STEM) images were recorded using an FEI Tecnai F20 TEM microscope, equipped with a high angle annular dark field (HAADF) detector, operated at 200 kV. For TEM analysis the NCs were dispersed in toluene and drop casted onto a carbon-coated copper grid. Field-emission scanning electron microscopy (SEM) was carried out on an Auriga Zeiss at 5.0 kV. Quantitative elemental analysis was performed by means of energy dispersive X-ray spectroscopy (EDX) within the SEM. Metal contents were determined with Perkin Elmer inductively coupled plasma (ICP) instruments using mass spectrometry (NexIon 350D) for Cs and atomic emission spectroscopy for Pb (Optima 8300). Samples synthesized in reactions with an upscaling factor of two for all substances were purified as reported earlier.[22] After the reaction the content of the flask was split into portions of 2 mL and centrifuged at 7000 rpm/6300 rcf for 15 minutes. After removing the supernatant 300 µL hexane were added to each portion. After re-dispersion of the particles 5 µL oleylamine and 5 µL oleic acid were added. After shaking the particles were precipitated with 300 µL of acetone and centrifuged for 3 minutes at 4400 rpm/2489 rcf. The precipitate was again re-dispersed with 300 µL of hexane and 3 µL of each ligand were added. After this the samples were precipitated again with acetone and dried. Of each purified and dried sample two aliquots of around 30 mg were digested by adding 5 mL of HNO_3 and 3 mL of H_2O_2 and heating until 210 °C in a microwave. Finally, the samples were diluted to 50 mL with ultrapure water and measured. For optical characterization the samples were diluted in hexane and analyzed using a quartz cuvette with 1 cm path length on a Cary 300 Bio UV-vis Spectrophotometer and a Cary Eclipse Fluorescence Spectrophotometer. Quantum yields were determined according to literature procedures using Rhodamine 6G and Fluorescein as standards.[33] Each QY was determined from measurements in three NC batches produced under the same conditions and with at least 2 measurements per batch. ATR-FTIR measurements were conducted with a Bruker alpha p instrument.

Nuclear Magnetic Resonance (NMR) measurements were recorded on a Bruker Avance III HD Spectrometer operating at a ^1H frequency of 500.26 MHz and equipped with a BBFO-Z probe. For NMR measurements batches scaled up with a factor 2 were produced and purified by two cycles of precipitation and re-

dispersion with acetonitrile/toluene before drying and redispersing them in deuterated toluene. The sample temperature was set to 298.2 K. One dimensional (1D) ^{1}H and 2D NOESY (Nuclear Overhauser Effect Spectroscopy) spectra were acquired using standard pulse sequences from the Bruker library. For the quantitative 1D ^{1}H measurements, 64k data points were sampled with the spectral width set to 20 ppm and a relaxation delay of 30 s. NOESY mixing time was set to 300 ms and 4096 data points in the direct dimension for 512 data points in the indirect dimension were typically sampled, with the spectral width set to 10 ppm. Diffusion measurements (2D DOSY) were performed using a double stimulated echo sequence for convection compensation and with monopolar gradient pulses.[34] Smoothed rectangle gradient pulse shapes were used throughout. The gradient strength was varied linearly from 2 to 95% of the probe's maximum value in 64 increments, with the gradient pulse duration and diffusion delay optimized to ensure a final attenuation of the signal in the final increment of less than 10% relative to the first increment. For 2D processing, the spectra were zero filled until a 4096−2048 real data matrix. Before Fourier transformation, the 2D spectra were multiplied with a squared cosine bell function in both dimensions, the 1D spectra were multiplied with an exponential window function. The diffusion coefficients were obtained by fitting the appropriate Stejskal- Tanner equation to the signal intensity decay.[34] Diffusion measurements (2D DOSY) were performed using a double stimulated echo sequence for convection compensation and with monopolar gradient pulses; dstegp2s.[35] Smoothed rectangle gradient pulse shapes were used throughout. The gradient strength was varied linearly from 2-95% of the probe's maximum value (calibrated at 50.2 G/cm) in 64 steps, with the gradient pulse duration and diffusion delay optimized to ensure a final attenuation of the signal in the final increment of less than 10% relative to the first increment. The diffusion coefficients were obtained by fitting the Stejskal-Tanner (ST) equation to the signal intensity decay. For the pulse sequence at hand, the appropriate ST equation is: [34]

$$I = I_0 e^{-(\gamma \delta g \xi)^2 D(\Delta - 0.6\delta)} \qquad (1)$$

with the gyromagnetic ratio of the observed ^{1}H nucleus γ, the gradient pulse length δ, the gradient strength g, the diffusion time Δ and the diffusion coefficient D. The shape factor ξ depends on the gradient shape but this is usually already corrected for in the gradient strength value by the Bruker software, TOPSPIN. The ST equation for other pulse programs is only slightly different and the impact on the diffusion coefficient is very small in the case of long diffusion times (Δ>250 ms). In a real DOSY experiment, values of Δ and δ are set while varying g to derive the decay curve.

LED testing: The measurements were carried out under ambient conditions. For green LEDs a Thorlabs' Mounted High-Power LED M365L2 UV pump with 0.55 W (3.42 V, I= 156.4 mA) was applied to illuminate the filter. The detection of the resulting luminescence was performed by means of an ISP 500 integrating sphere and a SPECTRO 320 PMT (Photomultiplier tube) based spectrometer, both from Instrument Systems. WLEDs were evaluated in an ISP 2000 integrating sphere coupled to a CAS 120 CCD-based spectrometer, both from Instrument Systems. The blue pump (450 nm) was run at 5.48 V and 58.8 mA, which implied a total power consumption of 0.31 W. The total irradiated filter area had a diameter of 25 mm. It is worth noticing that the switch from 365 nm to 450 nm as pump wavelength responded to the necessity of complementing the emission from the filter (by covering the short wavelength range) in the research of white light. In addition, it should be noted that both spectrophotometric systems are equivalent. The change from one system to the other is related to the fact that the housing of the 450 nm LED lamp is mechanically better adapted to ISP 2000 sphere ports.

3. Results and discussion

Figure 1 shows representative TEM micrographs of the cubic green-emitting $CsPbBr_3$ and cubic/partially squared orange-red-emitting $CsPbBr_{1.6}I_{1.4}$ NCs obtained in the presence of PMA ($CsPbX_3$-PMA) following the procedure described above. Based on the method of Protesescu *et al.* Cs-oleate in octadecene was injected to a hot solution of $PbBr_2$ or a mixture of $PbBr_2$ and PbI_2 in octadecene, oleylamine and oleic acid.[1] PMA was added before the injection. Figure 1C and 1D respectively show an atomic resolution HAADF STEM micrograph of one NC and its corresponding power spectrum, confirming the cubic crystal structure of the NC. The prepared $CsPbX_3$-PMA NCs thus exhibited the same crystal structure and a very similar emission maximum as those prepared in the same conditions by the unmodified synthesis protocol. $CsPbBr_3$-PMA and $CsPbBr_{1.6}I_{1.4}$-PMA NCs had average edge lengths of 9 ± 1 nm and 11 ± 2 nm outside the quantum confinement regime,[1] first absorption maxima at 504 and 561 nm and corresponding emission wavelengths of 513 and 586 nm.

SEM–EDX and ICP analyses revealed the $CsPbX_3$-PMA NCs to have slightly non-stoichiometric compositions, with an excess of lead and halide providing atomic ratios Cs:Pb:Br = 1:1.2:4 for green-emitting NCs and Cs:Pb:Br:I = 1:1.1:2:1.4 for orange-red NCs (see Supporting Information sections 2 and 3 for details). This off-stoichiometry may arise from the fact that the reaction is carried out under an excess of the two elements which may entangle with the polymer. An excess of halide may further be attributed to its role in the surface capping of the NCs, where it constitutes the negative counterpart of oleylammonium ions that stabilize the NCs in solution.[22] The NC quantum yield (QY) increased slightly but reproducibly with the polymer addition for both the green-emitting $CsPbBr_3$ NCs, from 49 ± 4 % to 53 ± 4 %, and the red-emitting $CsPbBr_{1.6}I_{1.4}$ NCs, from 84 ± 3 % to 88 ± 1 %. We believe the reason behind this slight increase to be a better passivation of the trap states by the more stable ligand shell.[22]

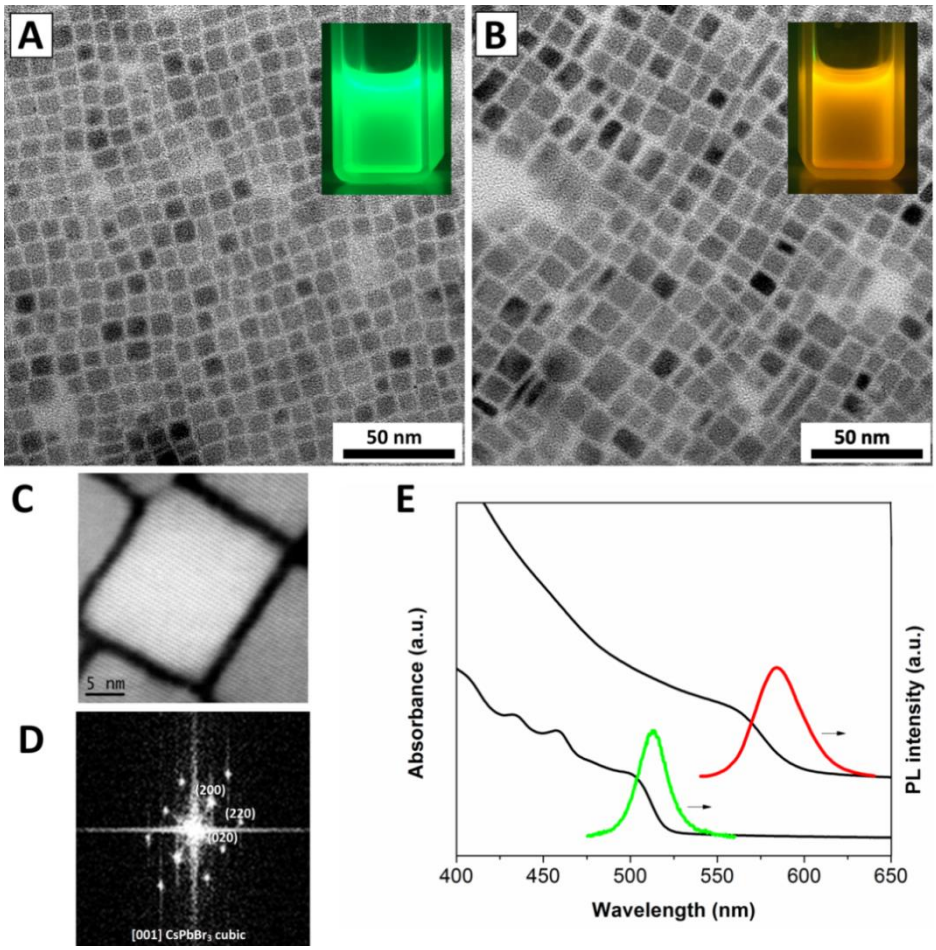

Figure 1. TEM micrographs of A) green $CsPbBr_3$ and B) orange $CsPbBr_{1.6}I_{1.4}$ NCs. C) Atomic resolution HAADF micrograph of one $CsPbBr_3$ NC and D) its power spectrum confirming a cubic crystal structure. E) Absorbance and emission spectra of the NCs in toluene solution.

To investigate this point further, we studied the composition of the ligand shell by means of ^{1}H solution NMR and IR spectroscopy (Figures S4 to S6). As reported earlier for pure $CsPbBr_3$ NCs,[22] the surface study by means of ^{1}H solution NMR showed the presence of oleylammonium bromide or oleylammonium oleate as surface ligands, in both the samples produced with and without the presence of PMA. The overlapping of the resonances between these ligands and the PMA prevented us to directly identify the presence of PMA in the ^{1}H NMR spectrum. Additionally, the similarity of the spectrum of PMA to the ligands and the fact that the anhydride ring seems to open during the reaction providing more -COOH and $–COO^-$ groups that are positioned close to oleic acid/oleate signals, further did not allow to unambiguously identify the presence of PMA on the samples by IR spectroscopy. However, Diffusion Ordered NMR Spectroscopy (DOSY) clearly revealed a change of the dynamic behaviour of those ligands in the presence of PMA. Lower diffusion coefficients and thus a solvodynamic radius closer to the NC size, were systematically obtained for all samples containing PMA (Table 1). This indicates that when polymer is added to the solution, ligands are indeed more tightly bound to the NCs. It furthermore indirectly proves the presence of PMA on the NC surface. While original ligands are still present, we presume that PMA is entangled on the ligand shell and acts as a contingency wall reducing the kinetics of the dynamic stabilization. On the other hand, NMR analysis showed that adding PMA after the synthesis was not so effective. Adding PMA to a pure $CsPbBr_3$ sample after the synthesis combined with sonication for 10 min and purification with acetonitrile resulted in larger diffusion coefficients when compared with purified samples synthesized in the presence of PMA

(Table 1). Besides, the addition of PMA under such circumstances presented a photoluminescence decay already visible by eye. This underlines the importance of adding PMA during the synthesis and not after. When reducing the amount of oleic acid added to the synthesis tenfold NCs produced by a reaction in presence of PMA exhibit a higher colloidal stability than those without and contain only small platelike crystals as side product while more than 100 nm sized plates are formed in the second case (see Figure S7). This means that PMA can either increase the solubility of the other reaction components or simply prevents weakly stabilized NCs to merge into larger structures.

Table 1. Comparison of diffusion coefficient and solvodynamic cube edges of $CsPbBr_3$ NCs produced with or without the presence of PMA with NC edge lengths determined from TEM micrographs.

Sample	Diffusion Coefficient ($\mu m^2\ s^{-1}$)	TEM size (nm)	Solvodynamic size (nm)
$CsPbBr_3$	89	9.4 ± 1.5	6.9
$CsPbBr_3$-PMA	64	9.7 ± 1.7	9.5
$CsPbBr_3$ (PMA)*	90	11 ± 2	6.8

* PMA added after synthesis

A main challenge to fabricate color conversion QD-WLEDs is to increase durability by preventing the NC degradation with a prolonged LED operation period. QD-LED degradation can be the result of a loss of QD luminescence when integrated into the device, due to photo-, thermal- or chemical degradation and to aggregation during processing due to incompatibility between the surface organic ligands and the polymer matrix. We tested the effect of the PMA on the stability of $CsPbX_3$ NCs when used as down converters of UV light. For this application, a toluene solution of $CsPbX_3$-PMA NCs was spread on 27 mm diameter glass substrates followed by slow evaporation of toluene in a semi-closed container to obtain a homogeneous layer.

These plates were placed on top of a commercial 365 nm UV-emitting LED delivering a radiometric power of 100 $mW_{opt.}$. Under these conditions the $CsPbBr_3$-PMA NCs emitted at 528 nm with a full-width at half maximum of 17 nm. The green-emitting LED without PMA had a color saturation of 0.944, a luminous efficacy of radiation of 255 $lm/W_{opt.}$ and a luminous efficacy of 2.5 $lm/W_{elec.}$ (1 $mW_{opt.}/W_{electr.}$). Devices incorporating $CsPbBr_3$-PMA NCs provided a color saturation increased to 0.988 and a much higher luminous efficacy of radiation up to 562 lm/W_{opt}, associated to the spectral proximity to the maximum of the photopic curve (683 $lm/W_{opt.}$, at 555 nm) and the partial UV light absorption by the polymer. The luminous efficacy was, in contrast, slightly lower, 1.8 $lm/W_{elec.}$.

Figure 2 shows the temporal evolution of the spectra obtained from two filters produced from the same amount of $CsPbBr_3$ NCs and thoroughly purified $CsPbBr_3$–PMA NCs under continuous illumination by a 365 nm pump in ambient conditions. This pump was operated at 58.8 mA forward current and provided an optical power of 100 $mW_{opt.}$ at sample level. In both cases, the luminescence decreased with time but only in case of the pure $CsPbBr_3$ sample shifted to longer wavelengths. The stability of the emission signal was significantly higher for the $CsPbBr_3$–PMA NCs, with 60% of peak area remaining after twelve operation hours, compared to $CsPbBr_3$ NCs with no PMA protection, decreasing down to 21%.

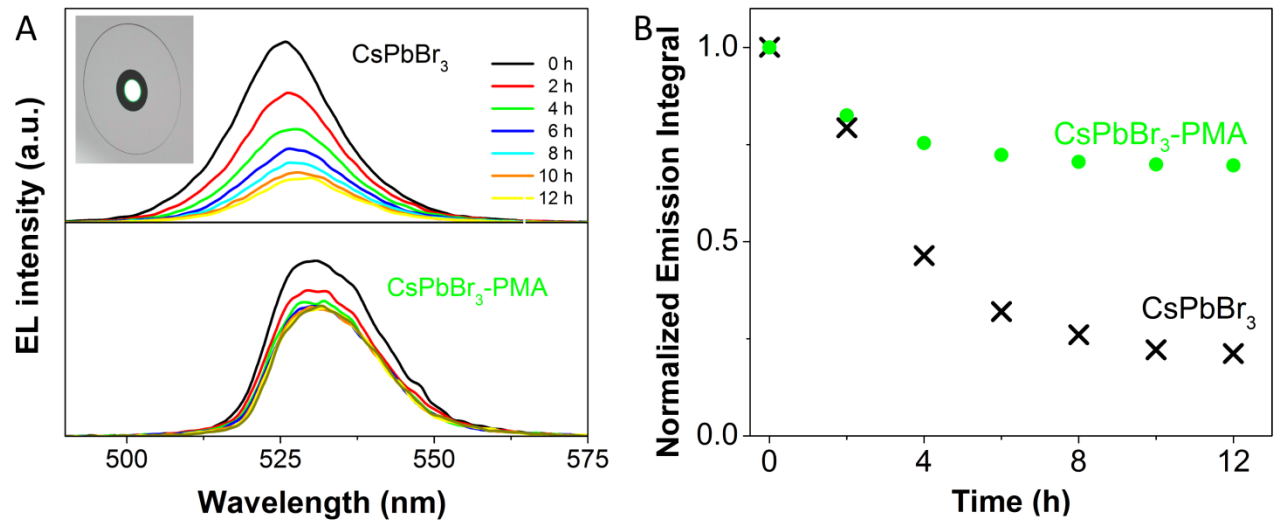

Figure 2. A) Temporal evolution of the emission spectra measured with filters of $CsPbBr_3$ and purified $CsPbBr_3$-PMA on a UV- LED with 100 mW at 365 nm with 58.8 mA forward current. The inset shows a green filter in the sample position of the integrating sphere. B) Normalized integrals of the emission peaks between 460 and 600 nm showing a three times lower decrease of the emission signal with PMA within twelve hours of constant irradiation.

X-ray diffraction (XRD) analysis (Figure 3) suggested that the NCs grow and partially rearrange crystallographically during long-term optical excitation. This growth and rearrangement was evidenced after 22 h operation for $CsPbBr_3$ NCs and after 3 days for $CsPbBr_3$–PMA NCs and was indicated by a narrowing of the XRD peaks following an extended illumination period. Growth and a rearrangement of the atoms through a phase transition would also explain the observed emission spectral red-shift. TEM micrographs in Figure S8 show the grown crystals. The polymer effectively slowed down these processes, but it did not completely prevent them.

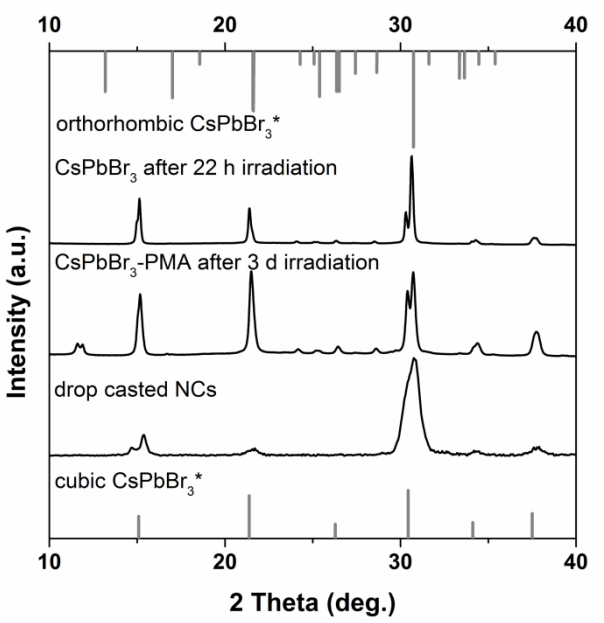

Figure 3. XRD patterns before and after long-term irradiation of 22 h ($CsPbBr_3$) and 3 days ($CsPbBr_3$-PMA). The initial NC deposited on a Si wafer by drop casting exhibit a cubic crystal structure with characteristically broad reflexes, no significant differences were observed for NC films with and without PMA. After the stability tests smaller peak widths indicate crystal growth and new peaks can be assigned to orthorhombic $CsPbBr_3$ (*references were calculated based on data from ref. [32], see experimental).

To investigate the performance of $CsPbX_3$ NCs in color conversion WLEDs, we combined green-emitting $CsPbBr_3$-PMA and red-emitting $CsPbBr_{1.6}I_{1.4}$-PMA NCs with emission peaks at 520 and 620 nm on independent free-standing plates. Owing to the sensitivity of perovskite NCs, a room temperature encapsulation and a remote-type architecture where a color conversion plate is placed on top of the LED at a distance was found to be more suitable for implementing perovskite-based color conversion LEDs.[36] NCs were embedded into a silicone matrix (Polastosil-2000) which was mixed with a catalyst at room temperature, spread on an optical glass substrate and left to cure. Heat-induced curing processes, widely applied in two-component silicone, proved inapplicable due to destruction of the perovskite NCs. To provide further protection from humidity and facilitate handling, the filter was covered by another glass layer when the silicone was mostly but not fully cured. The applied silicone is not only an easy to handle as well as cost effective matrix but also through adhesion forces towards the glass leads to a homogeneous distribution of the layer without any bubbles. Epoxy curing was not compatible with the NCs, as the NCs degraded upon contact with the resin, most likely due to unfavorable reactions with hydroxyl groups. Sandwiching the layers between glasses further opens the possibility of totally sealing the NCs and prevents any release of toxic Pb compounds. Apart from these design considerations, we discarded the blending of the two types of NCs in the same layer due to fast composition equilibration in solution that is not prevented by the ligand keeping but ion permeable PMA (see Supporting Information, Figure S9). Instead we sandwiched the NCs in silicone curing between two glass plates or stacks of two layers between three glass slides. Each silicone layer between two glasses was measured to cause a loss of optical emission of about 6%, part of this amount of light could be gained with modified LED design that redirects backscattered light in combination with more specific curing strategies reducing the difference in refractive indexes.

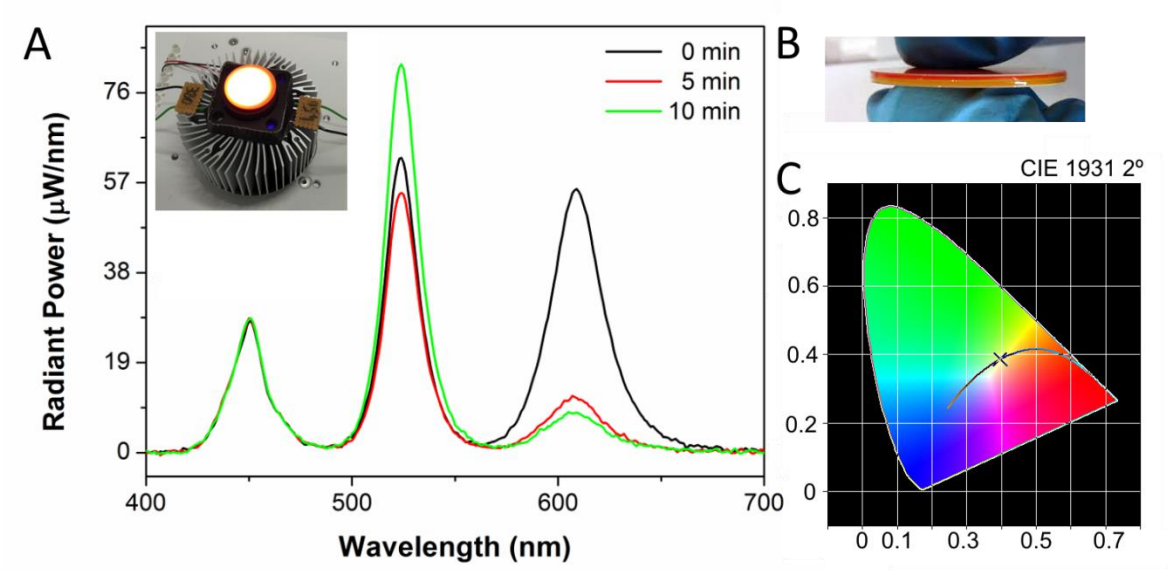

Figure 4. A) Electroluminescence spectra of a $CsPbX_3$–PMA WLED with an initial of CRI 72.4 and CCT of 3665 K. The inset shows a photograph of the device in the measurement set-up. B) Photograph of the stacked color conversion plates. C) CIE chromaticity diagram.

Color conversion plates containing the $CsPbX_3$-PMA NCs were mounted over a blue-emitting 446 nm pump. The maximum current, 58.8 mA providing 100 $mW_{opt.}$, was applied to test the device stability. Figure 4 shows the electroluminescence spectra obtained in ambient conditions of a WLED having the red-emitting filter stacked on top of the green-emitting one with one glass slide in between. The initial luminous efficacy of radiation (LER) of the WLED was 353 lm/W_{Opt}, which is within the range for optimum white light generation.[15] However, the luminous efficacy in terms of conversion of electricity into light (LE) of 4.5 $lm/W_{elec.}$ leaves room for improvement. Within 5 minutes the color temperature shifted from warm/neutral white light with 3665 K to 9300 K and the CRI decreased from 72.4 to 66.9 as a consequence of the degradation of the red component. Even with the improvement accomplished by the presence of the protecting PMA, in ambient conditions and with a relatively high forward current of 58.8 mA, the unstable red component limited the device durability. In iodide-based perovskite NCs photo activated atomic rearrangement is facilitated by the higher energetic gain of transition between the highly emissive cubic and less active tetragonal and orthorhombic phase of crystals containing iodine.[1,7,37,38] The reason for this lies in the intrinsic properties of the anions. The lower electronegativity of iodine and its larger size makes it less stable in the cubic $CsPbX_3$ structure, and thus the iodide-containing perovskite rearranges and decomposes faster than the bromide based one. In thin films recent studies show that doping $CsPbI_3$ with chloride ions improves the stability of the optically active perovskite crystal phase.[39] So far, solution based doping of iodide containing NCs has proven evasive but future advances in this direction may help to amend the instability of the red component. During irradiation the emission of the green filter increased as the red component decreased, indicating a substantial re-absorption of the emitted green light by the red component that may be solved by advanced filter design.

Figure 5 displays the EL spectra of a $CsPbX_3$–PMA WLED with higher red content under different driving currents ranging from 5 to 60 mA taken over a period of time of 6 minutes. A non-linear increase of the red component was observed, caused by simultaneous degradation that counteracts the trend of increasing

emission with higher currents. This again points out the vulnerability of the red component in comparison to the green one but on the other hand confirms the reliability of the green layer.

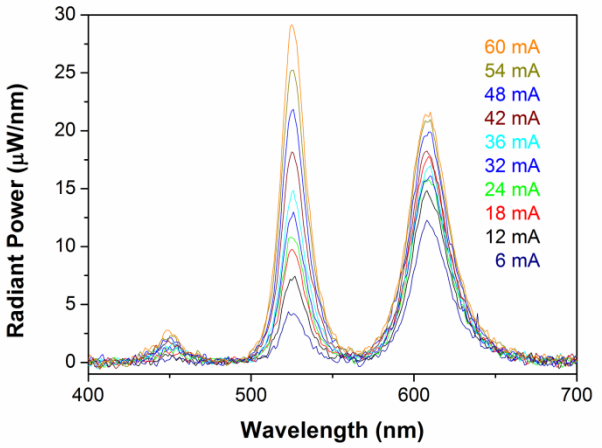

Figure 5. Electroluminescence spectra of a $CsPbX_3$– PMA WLED with increasing applied current.

4. Conclusions

$CsPbX_3$ NCs were synthesized in the presence of PMA. The addition of the polymer led to an increase of QY and optical stability of $CsPbX_3$ NCs under illumination in ambient conditions which is associated to a tighter bonding of the ligands in the presence of PMA as observed by ^{1}H NMR spectroscopy. Owing to the choice of emission wavelengths and the small emission bandwidths of these NCs, color conversion LEDs with high luminous efficacies of radiation and thus bright colors were achieved. The initial values of warm/neutral white light obtained are promising, although the bottleneck of an all-$CsPbX_3$ color converter WLED is the orange or red component obtained with a mixed bromide/iodide composition, which even in the presence of PMA shows a limited lifetime. While further advances in NC surface passivation in combination with component encapsulation strategies and advanced LED designs are necessary, our approach suggests that growing the NCs with a compatible polymer *in situ* during the reaction can facilitate their further processing and may be the key for further stabilization and encapsulation procedures.

Supporting Information

A visual assessment of the improved stability in ambient conditions, EDX and elemental analysis data, infrared spectra, 1 and 2D NMR spectra, additional TEM micrographs, a true color image of red and green samples with the product of mixing in solution and LED measurements with blank silicone/glass filter are supplied as Supporting Information.

Acknowledgments

This work was supported by the European Regional Development Funds, the Framework 7 program under project UNION (FP7-NMP-2012-310250) and HI-LED (FP7-ICT-2013-11-619912) as well as the Spanish MINECO Projects BOOSTER (ENE2013-46624-C4-3-R) and AMALIE (TEC2012–38901-C02–01). M.M. thanks the Spanish MINECO for financial support through the Juan de la Cierva-formación program. A.G. and J.A. acknowledge funding from Generalitat de Catalunya 2014 SGR 1638 and the Spanish MINECO MAT2014-51480-ERC (e-ATOM) and Severo Ochoa Excellence Program. We would like to thank Pablo Guardia for fruitful discussions.

References

(1) Protesescu, L.; Yakunin, S.; Bodnarchuk, M. I.; Krieg, F.; Caputo, R.; Hendon, C. H.; Yang, R. X.; Walsh, A.; Kovalenko, M. V. Nanocrystals of Cesium Lead Halide Perovskites ($CsPbX_3$, X = Cl, Br, and I): Novel Optoelectronic Materials Showing Bright Emission with Wide Color Gamut. *Nano Lett.* **2015**, *15*, 3692–3696.

(2) Yakunin, S.; Protesescu, L.; Krieg, F.; Bodnarchuk, M. I.; Nedelcu, G.; Humer, M.; De Luca, G.; Fiebig, M.; Heiss, W.; Kovalenko, M. V. Low-Thresold Amplified Spontaneous Emission and Lasing from Colloidal Nanocrystals of Caesium Lead Halide Perovskites. *Nat. Commun.* **2015**, *6*, 8056.

(3) Ramasamy, P.; Lim, D.-H.; Kim, B.; Lee, S.-H.; Lee, M.-S.; Lee, J.-S. All-Inorganic Cesium Lead Halide Perovskite Nanocrystals for Photodetector Applications. *Chem. Commun.* **2016**, *52*, 2067–2070.

(4) Bai, S.; Yuan, Z.; Gao, F. Colloidal Metal Halide Perovskite Nanocrystals: Synthesis, Characterization, and Applications. *J. Mater. Chem. C* **2016**, *4*, 3898–3904.

(5) Wang, Y.; Li, X.; Zhao, X.; Xiao, L.; Zeng, H.; Sun, H. Nonlinear Absorption and Low-Threshold Multiphoton Pumped Stimulated Emission from All-Inorganic Perovskite Nanocrystals. *Nano Lett.* **2016**, *16*, 448–453.

(6) Rainò, G.; Nedelcu, G.; Protesescu, L.; Bodnarchuk, M. I.; Kovalenko, M. V; Mahrt, R. F.; Stöferle, T. Single Cesium Lead Halide Perovskite Nanocrystals at Low Temperature: Fast Single-Photon Emission, Reduced Blinking, and Exciton Fine Structure. *ACS Nano* **2016**, *10*, 2485–2490.

(7) Seth, S.; Mondal, N.; Patra, S.; Samanta, A. Fluorescence Blinking and Photoactivation of All-Inorganic Perovskite Nanocrystals $CsPbBr_3$ and $CsPbBr_2I$. *J. Phys. Chem. Lett.* **2016**, *7*, 266–271.

(8) Swarnkar, A.; Chulliyil, R.; Ravi, V. K.; Irfanullah, M.; Chowdhury, A.; Nag, A. Colloidal $CsPbBr_3$ Perovskite Nanocrystals: Luminescence beyond Traditional Quantum Dots. *Angew. Chem., Int. Ed.* **2015**, *54*, 15424–15428.

(9) Sun, S.; Yuan, D.; Xu, Y.; Wang, A.; Deng, Z. Ligand-Mediated Synthesis of Shape-Controlled Cesium Lead Halide Perovskite Nanocrystals via Reprecipitation Process at Room Temperature. *ACS Nano* **2016**, *10*, 3648–3657.

(10) Nedelcu, G.; Protesescu, L.; Yakunin, S.; Bodnarchuk, M. I.; Grotevent, M. J.; Kovalenko, M. V. Fast Anion-Exchange in Highly Luminescent Nanocrystals of Cesium Lead Halide Perovskites ($CsPbX_3$, X = Cl, Br, I). *Nano Lett.* **2015**, *15*, 5635–5640.

(11) Zhang, D.; Eaton, S. W.; Yu, Y.; Dou, L.; Yang, P. Solution-Phase Synthesis of Cesium Lead Halide Perovskite Nanowires. *J. Am. Chem. Soc.* **2015**, *137*, 9230–9233.

(12) Akkerman, Q. A.; Innocenzo, V. D.; Accornero, S.; Scarpellini, A.; Petrozza, A.; Prato, M.; Manna, L. Tuning the Optical Properties of Cesium Lead Halide Perovskite. *J. Am. Chem. Soc.* **2015**, *137*, 10276–10281.

(13) Bekenstein, Y.; Koscher, B. A.; Eaton, S. W.; Yang, P.; Alivisatos, A. P. Highly Luminescent Colloidal Nanoplates of Perovskite Cesium Lead Halide and Their Oriented Assemblies. *J. Am. Chem. Soc.* **2015**, *137*, 16008–16011.

(14) Shamsi, J.; Dang, Z.; Bianchini, P.; Canale, C.; Di Stasio, F.; Brescia, R.; Prato, M.; Manna, L. Colloidal Synthesis of Quantum Confined Single Crystal $CsPbBr_3$ Nanosheets with Lateral Size Control up to the Micrometer Range. *J. Am. Chem. Soc.* **2016**, *138*, 7240–7243.

(15) Erdem, T.; Demir, H. V. Color Science of Nanocrystal Quantum Dots for Lighting and Displays. *Nanophotonics* **2013**, *2*, 57–81.

(16) Zhang, X.; Lin, H.; Huang, H.; Reckmeier, C.; Zhang, Y.; Choy, W. C. H.; Rogach, A. L. Enhancing the Brightness of Cesium Lead Halide Perovskite Nanocrystal Based Green Light-Emitting Devices through the Interface Engineering with Perfluorinated Ionomer. *Nano Lett.* **2016**, *16*, 1415–1420.

(17) Song, J.; Li, J.; Li, X.; Xu, L.; Dong, Y.; Zeng, H. Quantum Dot Light-Emitting Diodes Based on Inorganic

Perovskite Cesium Lead Halides ($CsPbX_3$). *Adv. Mater.* **2015**, *27*, 7162–7167.

(18) Li, X.; Wu, Y.; Zhang, S.; Cai, B.; Gu, Y.; Song, J.; Zeng, H. CsPbX3 Quantum Dots for Lighting and Displays : Room-Temperature Synthesis, Photoluminescence Superiorities, Underlying Origins and White Light-Emitting Diodes. *Adv. Funct. Mater.* **2016**, *26*, 2435–2445.

(19) Palazon, F.; Akkerman, Q. A.; Prato, M.; Manna, L. X-Ray Lithography on Perovskite Nanocrystals Films: From Patterning with Anion-Exchange Reactions to Enhanced Stability in Air and Water. *ACS Nano* **2016**, *10*, 1224–1230.

(20) Huang, H.; Chen, B.; Wang, Z.; Hung, T. F.; Susha, A.; Zhong, H.; Rogach, A.; Sci, C.; Huang, H.; Chen, B.; Wang, Z.; Hung, T. F.; Susha, A. S.; Zhong, H.; Rogach, A. L. Water Resistant $CsPbX_3$ Nanocrysals Coated by Polyhedral Oligomeric Silsesquioxane and Their Use as Solid State Luminophores in All-Perovskite White Light Emitting Devices. *Chem. Sci.* **2016**, DOI:10.1039/C6SC01758D.

(21) Kim, Y.; Yassitepe, E.; Voznyy, O.; Comin, R.; Walters, G.; Gong, X.; Kanjanaboos, P.; Nogueira, A. F.; Sargent, E. H. Efficient Luminescence from Perovskite Quantum Dot Solids. *ACS Appl. Mater. Interfaces* **2015**, *7*, 25007–25013.

(22) De Roo, J.; Ibáñez, M.; Geiregat, P.; Nedelcu, G.; Walravens, W.; Maes, J.; Martins, J. C.; Driessche, I. Van; Kovalenko, M. V; Hens, Z. Highly Dynamic Ligand Binding and Light Absorption Coefficient of Cesium Lead Bromide Perovskite Nanocrystals. *ACS Nano* **2016**, *10*, 2071–2081.

(23) Pathak, S.; Sakai, N.; Wisnivesky, F.; Rivarola, R.; Stranks, S. D.; Liu, J.; Eperon, G. E.; Ducati, C.; Wojciechowski, K.; Gri, J. T.; Haghighirad, A. A.; Pellaroque, A.; Friend, R. H.; Snaith, H. J. Perovskite Crystals for Tunable White Light Emission. *Chem. Mater.* **2015**, *27*, 8066–8075.

(24) Pan, J.; Sarmah, S. P.; Murali, B.; Dursun, I.; Pen, W.; Parida, M. R.; Liu, J.; Sinatra, L.; Alyami, N.; Zhao, C.; Alarousu, E.; Ng, T. K.; Ooi, B. S.; Bakr, O. M.; Mohammed, O. F. Air-Stable Surface-Passivated Perovskite Quantum Dots for Ultra-Robust, Single- and Two-Photon-Induced Amplified

Spontaneous Emission. *J. Phys. Chem. Lett.* **2015**, *6*, 5027–5033.

(25) Gonzalez-Carrero, S.; Galian, R. E.; Pérez-Prieto, J. Maximizing the Emissive Properties of $CH_3NH_3PbBr_3$ Perovskite Nanoparticles. *J. Mater. Chem. A* **2015**, *3*, 9187–9193.

(26) Song, W.; Yang, H. Efficient White-Light-Emitting Diodes Fabricated from Highly Fluorescent Copper Indium Sul Fi de Core/Shell Quantum Dots. *Chem. Mater.* **2012**, *24*, 1961–1967.

(27) Kim, H.; Kwon, B.-H.; Suh, M.; Kang, D. S.; Kim, Y.; Jeon, D. Y. Degradation Characteristics of Red Light-Emitting $CuInS_2$/ZnS Quantum Dots as a Wavelength Converter for LEDs. *Electrochem. Solid-State Lett.* **2011**, *14*, K55–K57.

(28) Ziegler, B. J.; Xu, S.; Kucur, E.; Meister, F.; Batentschuk, M.; Gindele, F.; Nann, T. Silica-Coated InP/ZnS Nanocrystals as Converter Material in White LEDs. *Adv. Mater.* **2008**, *20*, 4068–4073.

(29) Song, W.; Kim, J.; Yang, H. Silica-Embedded Quantum Dots as Downconverters of Light-Emitting Diode and Effect of Silica on Device Operational Stability. *Mater. Lett.* **2013**, *111*, 104–107.

(30) Di Corato, R.; Quarta, A.; Piacenza, P.; Ragusa, A.; Figuerola, A.; Buonsanti, R.; Cingolani, R.; Manna, L.; Pellegrino, T. Water Solubilization of Hydrophobic Nanocrystals by Means of Poly(maleic Anhydride-Alt-1-Octadecene). *J. Mater. Chem.* **2008**, *18*, 1991–1996.

(31) Bigall, N. C.; Curcio, A.; Leal, M. P.; Falqui, A.; Palumberi, D.; Di Corato, R.; Albanesi, E.; Cingolani, R.; Pellegrino, T. Magnetic Nanocarriers with Tunable pH Dependence for Controlled Loading and Release of Cationic and Anionic Payloads. *Adv. Mater.* **2011**, *23*, 5645–5650.

(32) Rodová, M.; Brožek, J.; Knížek, K.; Nitsch, K. Phase Transitions in Ternary Caesium Lead Bromide. *J. Therm. Anal. Calorim.* **2003**, *71*, 667–673.

(33) Grabolle, M.; Spieles, M.; Lesnyak, V.; Gaponik, N. Determination of the Fluorescence Quantum Yield of Quantum Dots: Suitable Procedures and Achievable Uncertainties. *Anal. Chem.* **2009**, *81*, 6285–6294.

(34) Sinnaeve, D. The Stejskal – Tanner Equation Generalized for Any Gradient Shape — An Overview of Most Pulse Sequences Measuring Free Diffusion. *Concepts Magn. Reson. Part A* **2012**, *40*, 39–65.

(35) Connell, M. A.; Bowyer, P. J.; Bone, P. A.; Davis, A. L.; Swanson, A. G.; Nilsson, M.; Morris, G. A. Improving the Accuracy of Pulsed Field Gradient NMR Diffusion Experiments: Correction for Gradient Non-Uniformity. *J. Magn. Reson.* **2009**, *198*, 121–131.

(36) Jang, E.; Song, W.; Lee, K.; Yang, H. Preparation of a Photo-Degradation- Resistant Quantum Dot – Polymer Composite Plate for Use in the Fabrication of a High-Stability White-Light-Emitting Diode. *Nanotechnology* **2013**, *24*, 045607.

(37) Lin, C. C.; Meijerink, A.; Liu, R. Critical Red Components for Next-Generation White LEDs. *J. Phys. Chem. Lett.* **2016**, *7*, 495–503.

(38) Young, J.; Rondinelli, J. M. Octahedral Rotation Preferences in Perovskite Iodides and Bromides. *J. Phys. Chem. Lett.* **2016**, *7*, 918–922.

(39) Dastidar, S.; Egger, D. A.; Tan, L. Z.; Cromer, S. B.; Dillon, A. D.; Liu, S.; Kronik, L.; Rappe, A. M.; Fafarman, A. T. High Chloride Doping Levels Stabilize the Perovskite Phase of Cesium Lead Iodide. *Nano Lett.* **2016**, *16*, 3563–3570.

Table of contents graphic